CARBON 50 (2012) 5232–5241

Available at www.sciencedirect.com

SciVerse ScienceDirect

journal homepage: www.elsevier.com/locate/carbon

Tunable uptake of poly(ethylene oxide) by graphite-oxide-based materials

Fabienne Barroso-Bujans [a,*], *Felix Fernandez-Alonso* [b,c], *Jose A. Pomposo* [a,d,e], *Eduardo Enciso* [f], *Jose Luis G. Fierro* [g], *Juan Colmenero* [a,e,h]

[a] *Centro de Física de Materiales-Material Physics Center (CSIC-UPV/EHU), Paseo Manuel Lardizábal 5, 20018 San Sebastián, Spain*
[b] *ISIS Facility, Rutherford Appleton Laboratory, Chilton, Didcot, Oxfordshire OX11 0QX, United Kingdom*
[c] *Department of Physics and Astronomy, University College London, Gower Street, London WC1E 6BT, United Kingdom*
[d] *IKERBASQUE-Basque Foundation for Science, Alameda Urquijo 36, 48011 Bilbao, Spain*
[e] *Departamento de Física de Materiales, Universidad del País Vasco (UPV/EHU), Apartado 1072, 20080 San Sebastián, Spain*
[f] *Departamento de Química Física I, Facultad de Ciencias Químicas, Universidad Complutense, 28040 Madrid, Spain*
[g] *Instituto de Catálisis y Petroleoquímica, CSIC, Marie Curie 2, Cantoblanco, 28049 Madrid, Spain*
[h] *Donostia International Physics Center (DIPC), Paseo Manuel Lardizábal 4, 20018 San Sebastián, Spain*

ARTICLE INFO

Article history:
Received 30 April 2012
Accepted 2 July 2012
Available online 7 July 2012

ABSTRACT

We investigate the role of structure and chemical composition on the uptake of poly(ethylene oxide) by a series of graphite oxides (GOs) and thermally reduced GOs, leading to the formation of polymer-intercalated GO and polymer-adsorbed graphene nanostructures. To this end, a series of poly(ethylene oxide) (PEO) - GO hybrid materials exhibiting a variable degree of GO oxidation and exfoliation has been investigated in detail using a combination of techniques including X-ray photoelectron spectroscopy, X-ray diffraction, thermogravimetry, scanning-electron microscopy, and nitrogen adsorption. Intercalation of the polymer phase into well-defined GO galleries is found to correlate well with both the degree of GO oxidation and with the presence of hydroxyl groups. The latter feature is an essential prerequisite to optimize polymer uptake owing to the predominance of hydrogen-bonding interactions between intercalant and host. Unlike the bulk polymer, these intercalation compounds show neither crystallisation nor glass-transition associated with the polymer phase. Exfoliation and reduction of GO result in high-surface-area graphene layers exhibiting the highest polymer uptake in these GO-based materials. In this case, PEO undergoes surface adsorption, where we observe the recovery of glass and melting transitions associated with the polymer phase albeit at significantly lower temperatures than the bulk.

1. Introduction

Graphite oxide (GO) offers unique opportunities associated with its subnanometer multilayer structure, hydrophilic character, and possibilities for the large-scale production of high-quality specimens. Although this material was first prepared well over a century ago, great efforts are nowadays devoted to understand its structure and composition as well as its thermal, electrical, and optical properties owing to its promising applications as graphene precursor [1]. GO exhibits excellent swelling and exfoliation behaviour very similar to what is found for clay minerals and metal-based graphite

* *Corresponding author:* Fax: +34 943015800.
E-mail address: fbarroso@ehu.es (F. Barroso-Bujans).
0008-6223/$ - see front matter
http://dx.doi.org/10.1016/j.carbon.2012.07.008

intercalation compounds. Unlike the case of layered silicates [2], a significantly smaller body of literature has been focused on the use of GO for polymer intercalation.

GO is highly hydrophilic as expected from its high oxygen content in the interlamellar regions. It can accommodate water or other solvent molecules (e.g. methanol, 1-propanol, benzene and $CHCl_3$) [3,4] between its layers with a surprisingly high degree of long-range order. GO can also accommodate cationic surfactants [5], alkylamines [6], alkylchlorosilanes [7] as well as macromolecular systems including high-molecular-weight polymers without inducing delamination of the GO layers. Matsuo et al. [8,9] were the first to prepare poly(ethylene oxide) (PEO)- and poly(vinyl alcohol) (PVA)-intercalated GO materials in alkaline aqueous media. This series of seminal studies demonstrated that these polymers penetrated the GO interlayer and formed stable compounds. The formation of sodium-hydroxide or copper-acetate colloidal particles was regarded as a prerequisite for the intercalation of mono or bilayers of PEO within the GO interlayer, respectively. Using Fourier-transform infrared spectroscopy (FTIR), these authors proposed zig-zag conformations for the PEO intercalant [10]. Unlike the intercalation of PEO into GO, they observed that the interlayer distance for intercalated PVA increased as a function of the polymer-to-GO ratio as a result of an inherent spread of polymer conformations within the interlayer. Matsuo et al. [8–10] also reported interlayer distances in the range 12.3–16.3 Å, whereas Bissessur and Scully [11] measured an interlayer spacing of 9.4 Å. It is now understood that such a difference in layer thickness was the result of the use of different synthetic routes to produce GO, as Matsuo et al. relied on a Brodie-based procedure [12] whereas Bissessur and Scully used the Hummers–Offeman method [13]. In addition, Matsuo et al. used sodium hydroxide and copper acetate to produce these intercalation compounds, whilst Bissessur and Scully used sodium hydroxide followed by successive washings with aqueous hydrochloric acid. Although none of these works clarify the effects of the metal cation on the intercalation process, it is very likely that the overall structure of GO is strongly dependent on the presence of these species as, for example, sodium hydroxide can be used quite effectively to reduce the oxygen content of GO [14]. Furthermore, the strong electrostatic interactions of PEO chains with mobile cations such as K^+, Li^+, and Na^+ are likely to dictate both the structural and dynamical behaviour of the intercalated polymer phase, as it is the case in clays and other layered minerals [15].

In a recent study [16], we have investigated the intercalation of PEO into GO as a function of intercalant molecular weight, as well as a function of host topology in the absence of NaOH [17]. GO synthesis was effected using a Brodie-based method to attain interlayer distances of 8.7–9.1 Å in the resulting PEO/GO intercalates. The expansion of the GO interlayer did not depend strongly on intercalant chain length, further reinforcing the notion that the oligomer and polymer chains adopt a planar conformation approaching atomic dimensions, i.e., well-defined and extreme 2D confinement. In addition, high-resolution inelastic neutron scattering (INS) unequivocally showed that the resulting zig-zag conformation of the intercalated species departs significantly from the characteristic 7_2 helical structure of the bulk crystal. These works demonstrated that polymer intercalation into GO constitutes an excellent platform for much-needed studies of macromolecular structure and dynamics under extreme two-dimensional confinement where the confined polymer shows a conspicuous absence of crystallization as well as the suppression of collective alpha-relaxation phenomena accompanied by a slow-down of local beta-relaxation processes in the dielectric response [18]. The primary advantage of using GO as a host material lies in the ability to control and tune its degree of oxidation and exfoliation [19] and, therefore, the strength of the interaction between host and intercalated species.

The present study explores the role of the chemical nature and composition of GO on polymer uptake leading to the formation of polymer-intercalated GO and polymer-adsorbed graphene nanostructures. To this end, we have prepared a series of PEO-GO hybrid materials with a variable degree of GO oxidation and exfoliation. Section 2 describes in detail our synthesis and characterization protocols. The GO materials and their associated polymer intercalates/adsorbates were characterized by X-ray photoelectron spectroscopy (XPS), elemental analysis (EA), nitrogen physisorption, X-ray diffraction (XRD), scanning electron microscopy (SEM), temperature-modulated differential scanning calorimetry (TM-DSC), and thermogravimetric analysis (TGA). Section 3 presents the main results of this study, including the chemical composition, structure, and morphology of the GO and thermally reduced GO, as well as of the polymer-intercalated GO and polymer-adsorbed graphene nanostructures. We close by summarizing the main findings of this work as well as by highlighting the need for both state-of-the-art synthesis protocols in conjunction with advanced characterization techniques so as to gain fresh insights into the nature of confined matter at the nanoscale.

2. Experimental

2.1. Materials

2.1.1. Synthesis and reduction of graphite oxide

GO was produced using natural graphite from Alfa Aesar, reference 40799, universal grade, 200-mesh, 99.9995% (metal basis). Graphite oxidation was achieved using a modified Brodie method [12,19]. Briefly, a reaction flask containing 200 mL of fuming nitric acid (Fluka) was cooled to 0 °C with a cryostat bath for 20 min, followed by the addition of 10 g of graphite. Next, 80 g of potassium chlorate (Fluka) was slowly added over a period of 1 h to avoid sudden increases in temperature. In order to vary the degree of oxidation of the GO samples, reaction times and temperatures were varied as reported in Table 1. To purify the final reaction product, the mixtures were diluted in distilled water and filtered until the supernatant had a nitrate content lower than 1 mg/L [AQUANAL-plus nitrate (NO_3) 1–50 mg/L]. The resulting GO slurry was dried at 80 °C for 24 h in a vacuum oven ($P < 0.1$ mbar) and stored in this oven at room temperature until further use.

Reduced graphite oxides (RGOs) were produced by thermal treatment of specimen GO(21;0) (cf. Table 1). RGO(2;200) and RGO(18;200) were heated at a rate of 10 °C/min from room

Table 1 – Elemental composition and oxygen-to-carbon atomic ratio (O/C) of GO, RGO, and G as a function of reaction conditions as determined by EA and XPS. Interlayer spacings (d) obtained from the (001) Bragg reflection are reported in the fourth column.

Sample	Time (h)	Temp. (°C)	d (Å)	C (at)	H (at)	O (at)	N (at)	O/C EA	O/C XPS
Chemical Oxidation Route									
GO(2;0)	2	0	5.6	8.00	1.08	2.29	0.06	0.286	0.338
GO(5;0)	5	0	5.6	8.00	1.02	2.42	0.05	0.303	0.321
GO(21;0)	21	0	5.7	8.00	1.14	2.72	0.03	0.340	0.364
GO(21;25)	21	25	5.8	8.00	1.13	3.09	0.03	0.386	0.363
GO(40;25)	40	25	5.8	8.00	1.51	3.23	0.01	0.403	0.374
Thermal Reduction Route									
RGO(2;200)[a]	2	200	5.5	8.00	0.81	2.37	0.02	0.297	0.337
RGO(18;200)[a]	18	200	5.5	8.00	0.39	2.00	0.01	0.250	0.271
RGO(600)[b]	–[c]	–[c]	3.5	8.00	0	1.05	0.02	0.132	0.116
G[b]	(1 min)	1000	3.5	8.00	0.11	1.04	0.02	0.130	0.127

[a] In vacuo.
[b] In Argon.
[c] Dynamic heating from room temperature to 600 °C at a rate of 1 °C/min.

temperature to 100 °C, followed by a ramp at 1 °C/min to the indicated temperature (200 °C). At this stage, the samples were heated for either 2 or 18 h. RGO(600) was obtained by heating GO from room temperature to 600 °C at 1 °C/min in a tube furnace under an Argon flux. Graphene-like sheets (specimen G in Table 1) were obtained by placing GO on a glass boat and inserting it into a quartz tube under an Argon flux. This tube was then loaded into a tube furnace preheated to 1000 °C. After 1 min, the tube was removed and cooled down to room temperature. The composition of the different GO samples and the oxygen-to-carbon atomic ratio (O/C) obtained by EA and XPS are shown in Table 1.

2.1.2. Polymer uptake

PEO (Aldrich) with a molecular weight Mn = 9.4×10^4 g/mol and polydispersity index 1.08 was used in all experiments. PEO uptake by the GO-based materials listed in Table 1 was performed in aqueous solution by stirring 0.5 g of PEO previously dissolved in 20 mL water with 0.5 g of GO, RGO, and G for 15 days. Hereafter, the resulting adducts are denoted as PEO/GO, PEO/RGO, and PEO/G. Excess PEO was removed by filtration and thorough aqueous washings. The resulting PEO/GO, PEO/RGO, and PEO/G were then dried at 80 °C for 24 h in a vacuum oven (P < 0.1 mbar) connected to a dry scroll rotatory pump. All samples were kept dry in the vacuum oven at room temperature before testing.

2.2. Characterization

2.2.1. X-ray photoelectron spectroscopy

XPS spectra were recorded using an Escalab 200R spectrometer equipped with a hemispherical analyzer and operated in a constant-pass energy mode with unmonochromatized MgKα X-ray radiation (hν = 1253.6 eV) powered at 10 mA and 12 kV. The binding energies (BE) were referenced to the C1s peak at 284.9 eV. Data processing was performed with the XPS Peak program. The spectra were decomposed with the least-squares fitting routine provided by the software using a Gauss/Lorentz product function and a Shirley background. Atomic ratios were calculated from background-subtracted peak areas using sensitivity factors provided by the data-analysis system.

2.2.2. X-ray diffraction

XRD patterns were measured using a Bruker D8 Advance powder diffractometer equipped with a CuKα radiation source (λ = 1.54 Å), a LynxEye detector and an Anton-Paar TTK450 temperature stage. The radiation source was operated at a generator voltage of 40 kV and a current of 40 mA. XRD data were collected at 25 °C over the angular range 2θ = 5–60° with a stepsize of 0.026° in Bragg–Brentano parafocusing geometry. Each diffractogram was measured over short intervals of ca. 110 s in order to ensure that the (highly hygroscopic) GO materials were not exposed to air for unnecessarily long periods of time. Under these experimental conditions, the resulting XRD data correspond to dry GO-based materials.

2.2.3. Thermogravimetry

Thermogravimetry (TGA) was carried out with a Q500 Thermogravimetric Analyzer from TA Instruments. Samples were heated from room temperature to 600 °C at a rate of 1 °C/min upon a constant N_2 flow of 60 mL/min. The amount of PEO in PEO/GO, PEO/RGO, and PEO/G was calculated from sample-residue analysis as described in [18]. Isotherms were collected at 200 °C using the following heating ramps: 10 °C/min from room temperature to 100 °C, followed by 1 °C/min up to the isothermal temperature.

2.2.4. Scanning electron microscopy

SEM images were recorded with a TM3000 Tabletop microscope from Hitachi in composition mode and operating at an accelerating voltage of 15 kV.

2.2.5. BET surface

Nitrogen adsorption isotherms at 77 K were obtained using the static volumetric method on an ASAP 2020 from Micromeritics. All samples were degassed at 95–180 °C for 3 h to a residual vacuum <10 μm Hg. Isotherms were analysed using the Brunauer–Emmett–Teller (BET) equation [20], and BET areas were calculated using a value of 0.162 nm for the

molecular radius of nitrogen [21]. Micropore areas were obtained from standard t-plots, where t is the statistical thickness of the adsorbed film calculated using the Harkins–Jura equation [22]. Pore-size distributions were obtained via the Barrett–Joyner–Halenda (BJH) method [23] on the adsorption branches of the isotherms assuming a cylindrical-pore model.

2.2.6. *Temperature-modulated differential scanning calorimetry*

DSC measurements were carried out on ~12 mg specimens using a Q2000 TA instrument in both standard and temperature-modulated (TM) modes. Standard DSC measurements were performed by placing the samples in sealed Aluminium pans, holding the temperature for 10 min at 353 K, and cooling to 100 K at the highest attainable cooling rate. Bulk PEO was melted on a hot plate at 353 K and quenched by immersing the sample in liquid nitrogen followed by insertion into the DSC cell at 100 K. After the cooling run, all samples were heated back to 353 K in TM mode with a 0.48 K temperature amplitude, 60 s modulation period, and 3 K/min underlying heating rate. A Helium flow rate of 25 mL/min was used all throughout.

3. Results and discussion

3.1. *Chemical composition of GO materials*

In order to produce GO materials with variable oxygen-to-carbon (O/C) ratios, two different synthetic routes were followed. The first route was chemical, whereby GOs with an increasing degree of oxidation were produced by increasing the time and temperature of oxidation. The second route was thermal, where GO was reduced and exfoliated by implementing different temperature programs under an inert atmosphere. Fig. 1a outlines both chemical and thermal routes and Table 1 provides a summary of all samples of relevance to this work specifying the temperature and time of reaction as well as their chemical composition obtained from EA and XPS measurements. As observed for the GO obtained by the chemical oxidation route, its composition is characterised by O/C ratios between 0.29–0.40, leading to interlayer distances from 5.6 to 5.8 Å.

The experimental protocol that defines our thermal reduction route (Fig. 1b) is based on our previous study of the thermal behaviour of GO using isothermal and dynamic thermogravimetry [19]. This study determined that the isothermal reduction of our Brodie-based GO followed two distinct kinetic mechanisms associated with either diffusion or autocatalytic decomposition. In the first process, carbon dioxide (CO_2) and water are released and diffuse within the interlayers virtually without altering the GO-layer stacking. In the second process, further heating leads to the production of CO_2 and water in large amounts, ultimately resulting in the exfoliation of GO sheets. To determine the time needed to reduce the graphite oxide at 200 °C following either of these two mechanisms, we performed isothermal thermogravimetric scans on sample GO(21;0) (cf. Table 1). Fig. 2 shows that the weight loss and the first thermogravimetric derivative exhibit the two processes discussed above. On the basis of these findings, isothermal treatments were carried out for periods of 2 and 18 h. In this manner, RGO(2;200) and RGO(18;200) were obtained by heating GO(21;0) at 200 °C for 2 or 18 h, a period after which the resulting O/C ratios decreased to 0.30 and 0.25, respectively. The interlayer distance as determined by XRD was 5.5 Å for both samples.

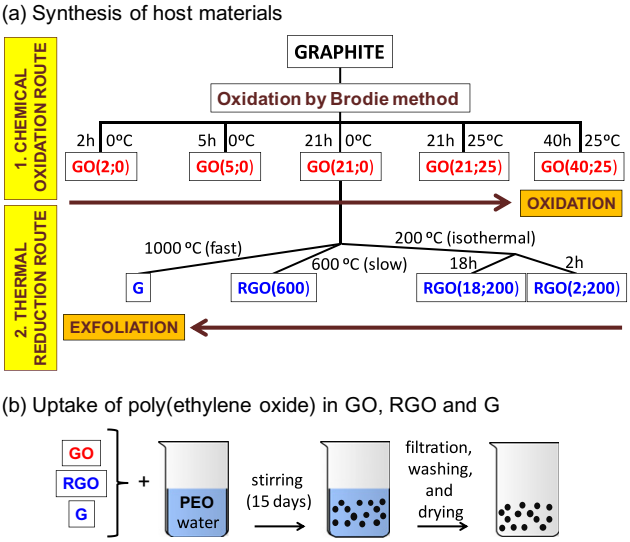

Fig. 1 – (a) Routes for the synthesis of GO materials: (1) Chemical oxidation route where GOs with an increasing degree of oxidation were produced from the oxidation of graphite by a modified Brodie method (different times and temperatures of reaction); (2) Thermal reduction route where GO(21;0) was heated with different temperature programs in isothermal and dynamic modes (fast and slow rates) to reduce and exfoliate GO. (b) Graphical summary of the laboratory procedure used to intercalate and/or adsorb PEO into GO-based materials.

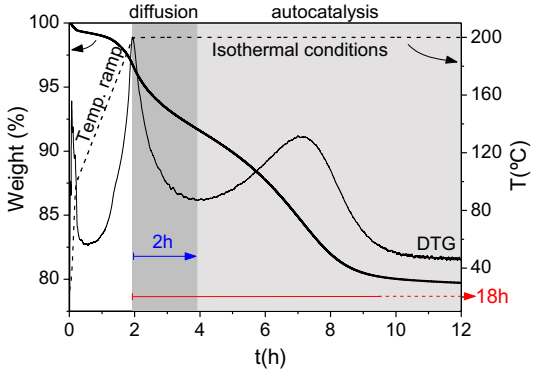

Fig. 2 – Isothermal thermogravimetric data for GO(21;0) at 200 °C (thick black line). These data were used to select the time corresponding to the reduction of GO following either diffusion-limited (2 h) or autocatalytic (18 h) kinetics. For more details on these kinetic mechanisms see [19]. Dashed line: temperature program. DTG: first derivative of the thermogravimetric data.

RGO(600) was obtained by dynamic heating at 1 °C/min from room temperature to 600 °C and sample G was obtained from rapid heating to 1000 °C, a process currently used to produce graphene-like sheets in large quantities for a variety of applications [1,24]. These samples showed the lowest oxygen content of the series amounting to an O/C ratio of 0.13.

As a result of these heating procedures, part of the oxygen in GO is removed leaving residual hydroxyl groups and other oxygen-containing moieties [25]. To determine the nature and relative amount of these functional groups in pristine and thermally reduced GO, samples were characterized by XPS. Table 1 shows the O/C ratios for the different GO hosts of relevance to this work as determined by this technique, which compare reasonably well with those determined by EA. Fig. 3 displays C1s XPS data for representative samples. All spectral peaks were decomposed into a linear combination of symmetric components. The XPS data for GO and RGO specimens were satisfactorily described by two and three distinct contributions, respectively, in agreement with the literature [25]. The peak at 284.8 eV corresponds to sp^2 C–C bonds in graphitic carbon whereas that at 286.5 eV is assigned to epoxy and hydroxyl C–O bonds. The third component at 287.7–288.3 eV in RGO specimens is assigned to carbonyl (C=O) groups. The C1 peak for G was adequately described by five components. In addition to the bands of native GO, we observe three peaks at 287.7, 289.3, and 291.3 eV. The two first peaks are assigned to C=O and carboxyl (COOH) species, respectively. The peak at 291.3 eV corresponds to the plasmon/shake-up satellite (π–π^* transition) of graphitic carbon.

The relative concentration of C–O bonds relative to C–C bonds increases by a factor of ~1.5 in going from GO(2;0) (0.89) to GO(40;25) (1.32) as a result of a higher extent of oxidation during synthesis. In the case of thermally reduced GO, this ratio is gradually reduced and it is accompanied by the appearance of new C=O groups in RGO and both C=O and COO groups in G, as a result of the rearrangement of hydroxyl, epoxy, and carbonyl groups upon heating [26]. Moreover, it is quite apparent that the rearrangement of these functional groups depends quite strongly on heating rate, an observation that is yet to be explored either via experiment or computer simulation.

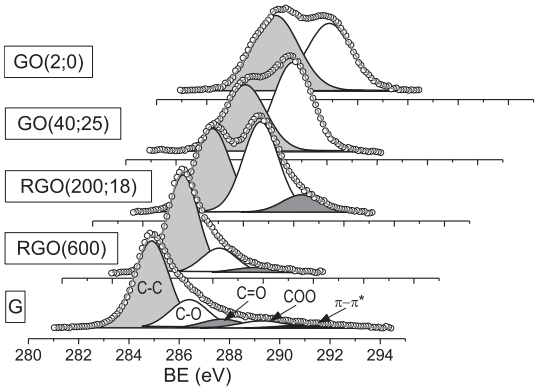

Fig. 3 – C1s core-level spectra of GO and thermally reduced GO. For more details on sample composition see Table 1.

3.2. *Structure and morphology of poly(ethylene oxide) nanostructures*

3.2.1. *Chemically modified graphite oxide*

PEO chains of molecular weight 94 kg/mol were intercalated into GO by diffusion in aqueous liquid media (see Fig. 1b). Such a process is facilitated by strong hydrogen-bonding interactions between the polymer and the GO. As a result, the PEO chains are strongly retained by GO and further PEO recovery following the intercalation process is not feasible. As shown in Fig. 4, the amount of intercalated PEO in chemically modified GO varies from 9 to 27 wt.% as the degree of oxidation is increased, ultimately reaching a maximum at an O/C ratio of ca. 0.38. From this point onwards, the amount of intercalated PEO undergoes, if anything, a slight decrease. These results indicate that the oxygen content in GO plays a central role in the intercalation of PEO chains. According to the model of Lerf et al. [27], GO is mainly decorated by tertiary alcohols and epoxy (1,2-ethers) on the basal planes. In our particular case, FTIR has been used in previous studies [16,18] to establish that hydrogen-bonding interactions occur predominantly between PEO ether groups and GO hydroxyls (OH), as expected on the grounds of their chemical structure. For long polymer chains, hydrogen bonds between OH end-groups of the polymer and both OH and epoxy groups in GO are also plausible, yet these can be neglected given their exceedingly low occurrence in high-molecular-weight PEO chains.

With these considerations in mind, the degree of interaction between PEO chains and the different GO hosts can be evaluated by calculating the molar content of oxygen in the polymer relative to OH in GO. The latter quantity has been estimated from the total hydrogen content in GO assuming that all hydrogen occurs in OH form. These data are shown in Fig. 5 and exhibit a very similar trend to that observed in Fig. 4, implying that the higher the amount of PEO in PEO/GO, the higher the amount of PEO oxygen per mol of OH in GO owing to a stronger interaction between the polymer and the host. Interestingly, these data reaches a maximum when the ratio of PEO oxygens to GO OH reaches unity, indi-

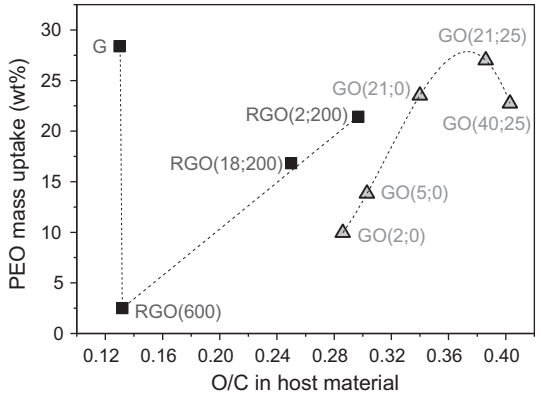

Fig. 4 – PEO mass uptake in chemically modified GO (triangles) and thermally modified RGO and G (squares) obtained from EA. Dashed lines are guides to the eye. For more details on sample composition, see Table 1.

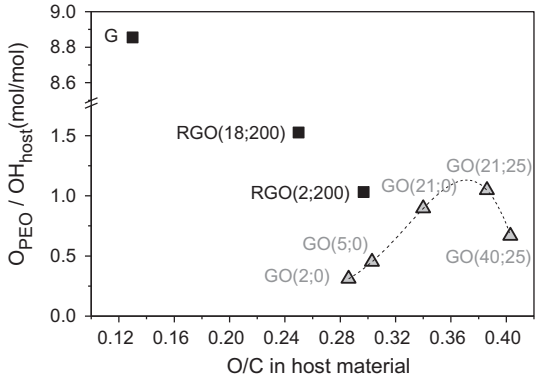

Fig. 5 – Molar ratio of PEO oxygen to OH groups in GO, RGO, and G as a function of O/C of the host obtained from EA. Dashed lines are guides to the eye. For more details on sample composition, see Table 1.

cating that in PEO/GO(21;25) each PEO oxygen atom corresponds to one OH group in the GO host. This result strongly suggests that the maximum amount of PEO chains in the GO interlayer is reached when the polymer - host interaction is maximised via hydrogen bonding interactions where PEO/GO acts as hydrogen acceptor/donor. It is somewhat surprising that a further increase in the amount of OH groups in the host does not translate into an increase in PEO uptake, as observed in sample PEO/GO(40;25) where the amount of intercalated PEO decreases to 23 wt.%. We surmise that this behaviour might be caused by changes in the morphology or chemical make-up of GO at these high levels of oxidation. Polymer uptake in thermally reduced GO is discussed in the next section.

Fig. 6 shows XRD data for representative PEO/GO and GO specimens. XRD data for bulk PEO are also included in this figure. The interlayer spacings for all GOs investigated in this work are also reported in Table 1. Graphite oxide is a paracrystalline material characterised by turbostratic layer stacking, i.e., irregular shifts and/or rotations of individual planes along the crystallographic *c*-axis. The layers are also irregular since epoxide and hydroxyl groups, as well as remaining C=C double bonds are not distributed evenly within a given two-dimensional layer. As a consequence, the XRD data display a prominent (001) reflection at 1.10 $Å^{-1}$ followed by a much weaker (002) Bragg reflection at 2.23 $Å^{-1}$ indicative of in-plane ordering [4]. Fig. 6 shows that the (001) Bragg reflection in GO shifts to slightly lower Q values as a function of the degree of oxidation, giving interlayer distances in the range 5.6–5.8 Å. Moreover, the absence of any remaining peaks associated with the starting graphite material even for the least-oxidized GO sample [GO(2;0)] indicate that all GO planes are oxidized.

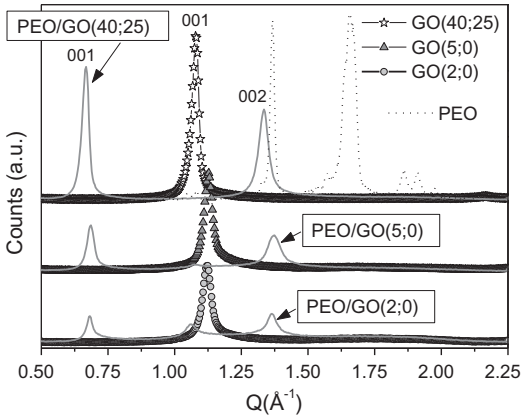

Fig. 6 – Representative XRD data of PEO/GO intercalates. The reaction time and temperature at which each GO sample was synthesized are indicated in brackets and are related to their corresponding degree of oxidation (see Table 1). For clarity of presentation, XRD profiles have been offset vertically by an arbitrary numerical constant. Dotted lines correspond to XRD data for bulk PEO.

Intercalated PEO/GO samples display XRD patterns with two well-defined (001) and (002) reflections, which account for the significant expansion of the GO interlayer along the crystallographic *c*-axis upon intercalation, from 5.6–5.8 to 9.1–9.5 Å. These data show a slightly shorter interlayer thickness for PEO/GO(2;0) and PEO/GO(5;0) (9.1 Å) compared to other PEO/GO composites [9.2 Å for PEO/GO(21,0), 9.4 Å for PEO/GO(21;25), and 9.5 Å for PEO/GO(40;25)], as expected given the slightly tighter interlayer distances of the starting GO(2;0) and GO(5;0) hosts (cf. Table 1). The presence of a Bragg peak at 1.06 $Å^{-1}$ for PEO/GO(2;0), corresponding to an interlayer spacing of 5.92 Å (close to that of GO), indicates that there exist regions in the sample where the polymer cannot intercalate and, therefore, remain empty. This result is in line with the lower amount of PEO content in GO(2;0) shown in Fig. 4. Moreover, the XRD pattern for bulk crystalline PEO shows well-defined and intense peaks at ~1.36 and ~1.66 $Å^{-1}$ arising from its well-known 7_2 helical structure. This structure is characterized by seven chemical units $–CH_2–CH_2–O–$ executing two turns with an angular period of 19.3° [28]. In our intercalation compounds, no diffraction features are observed which can be assigned to crystalline PEO. This finding is most evident in PEO/GO(40;25), whose (002) reflection at 1.33 $Å^{-1}$ does not overlap with that of the PEO crystal at ~1.36 $Å^{-1}$. In the case of PEO/GO(5;0) and PEO/GO(2;0), the (002) reflection does appear at ~1.36 $Å^{-1}$, yet no Bragg reflections around 1.66 $Å^{-1}$ attributable to bulk PEO have been observed. These results are a strong indicator that the polymer chains inside the GO interlayer remain amorphous.

3.2.2. *Thermally reduced graphite oxide*

Similar experimental procedures to those used for the intercalation of PEO in GO were used to produce PEO/RGO and PEO/G samples. The amounts of PEO absorbed in thermally reduced GO as a function of O/C ratio are shown in Fig. 4. In this case, the amount of absorbed PEO decreases with decreasing oxygen content in RGO samples from RGO(2;200) to RGO(600) and it increases quite significantly in PEO/G. When a comparison is made in terms of the molar ratio of PEO oxygen per mol of host OH (see Fig. 5), a different trend is observed. Interestingly, the PEO-oxygen-to-host-hydroxyl ratio in the thermally reduced GO samples was ≥1 and increased noticeably with the degree of reduction [note that for RGO(600), the amount of hydrogen is zero and, therefore, no OH groups are present in the sample]. A value of unity for this ratio implies maximal interaction via hydrogen bonds

between intercalate and host. With this picture in mind, values >1 denote a regime of saturation whereby there exist more PEO oxygen atoms per host OH. PEO/G displays an exceedingly high value for this ratio (8.9) indicating the highest level of saturation of the series. Somewhat surprisingly, this sample also exhibits the highest amount of absorbed polymer (28 wt.%). To explain these results, the XRD data of RGO, G, PEO/RGO, and PEO/G samples as well as the SEM images of PEO/RGO and PEO/G shown in Fig. 7 must be examined in closer detail. To facilitate comparison, XRD and SEM data of the precursor GO(21;0) are also presented in this figure.

The SEM images shown in Fig. 7 demonstrate that the overall morphology of all PEO/GO-based materials studied in this work is dominated by the presence of the graphitic matrix, a result which is consistent with its dominant abundance relative to the polymer phase. Furthermore, comparison of these SEM data with that of bulk PEO (cf. Fig. S1) also confirms the absence of the latter in our specimens. The heat treatment applied to GO at 200 °C for 2 h and 18 h appear not to cause GO exfoliation, as can be deduced from the intense (001) diffraction peak at $Q = 1.15\ Å^{-1}$ for RGO(2;200) and RGO(18;200) shown in Fig. 7, although in the latter sample the SEM image reveals the presence of expanded zones resembling accordion-like structures. On the other hand, the slow dynamic heating of GO to 600 °C gave rise to an exceedingly low concentration of oxygen, similar to that of G (Table 1) yet structurally very different. Both RGO(600) and G are characterised by a broad diffraction feature around $1.8\ Å^{-1}$, corresponding to a characteristic pair-correlation distance of ~3.5 Å, in reasonable agreement with the interlayer distance in pristine graphite (3.4 Å), and clearly affected by disorder at the atomic scale. This result is suggestive of a significant restacking of graphite planes upon heating [19]. However, the SEM images of both RGO and G reveal a distinct stacking for both materials, namely, RGO showing densely packed sheets and G exhibiting fluffy and accordion-like structures.

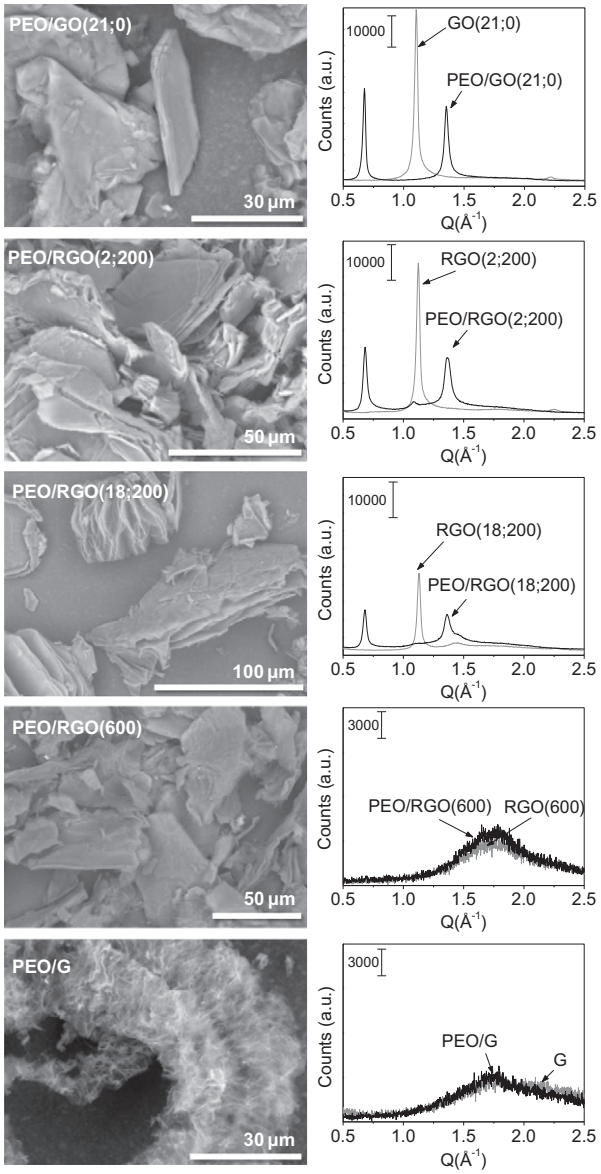

Fig. 7 – Left: SEM micrographs of PEO/GO(21;0), PEO/RGO(2;200), PEO/RGO(18;200), and PEO/G samples. Right: corresponding XRD patterns. For comparison, the XRD data of GO(21;0), RGO(2;200), RGO(18;200), and G are shown using grey symbols (for more details see Table 1).

The XRD diffraction patterns of PEO/RGO(2;200) and PEO/RGO(18;200) shown in Fig. 7 show (001) and (002) reflections at 0.68 and $1.36\ Å^{-1}$, respectively, as in PEO/GO(21;0), indicating that PEO chains are intercalated in an interlayer space of 9.2 Å. This is not the case for PEO/RGO(600) and PEO/G, in which the diffractograms do not show any changes with respect to the bare substrate. This result suggests that PEO chains cannot enter the interlamellar regions and remain absorbed in the external surface of RGO(600) and G samples with an uptake of 2.5 wt.% and 28 wt.%, respectively.

To gain further insight into the morphology and texture of RGO and G samples, BET surface areas, micropore areas, pore volumes, and average pore diameters for RGO(18;200), RGO(600), G, and their corresponding GO precursors were obtained from an analysis of nitrogen adsorption–desorption isotherm data collected at 77 K (cf. Table 2). Isotherms and pore-size distributions are reported in the Supplementary Information (see Figs. S2 and S3, respectively). All data conform to a type-IV isotherm characterized by a broad pore-size distribution. Moreover, these data indicate the occurrence of multilayer adsorption at low pressures and nitrogen condensation inside the matrix pores, as evidenced by an enhancement of nitrogen adsorption at a reduced pressure of 0.4. A large hysteresis denotes the presence of small pores that block the escape of nitrogen molecules from some large pores. However, only G shows a high surface area ($632\ m^2/g$), a moderate micropore area ($55\ m^2/g$), and a high mesoporous pore volume ($3.6\ cm^3/g$). For sample G, the fast annealing of GO at 1000 °C represents the key factor leading to the presence of nano/micropores. However, the micropore area amounts to just 9% of the total BET area, indicating that the amount of gas adsorbed in those micropores is negligibly small. Sample G is characterized by a large available surface area capable of accommodating significant amounts of PEO. Moreover, although the average pore diameter obtained for the G sample from the adsorption branch of the isotherm

Table 2 – Average surface areas, pore volumes, and pore diameters obtained from an analysis of nitrogen-adsorption isotherm data as detailed in the text.

Host materials	BET Area (m^2/g)	Micropore Area (m^2/g)	V_{meso}(BJH) (cm^3/g)	Average pore diameter (nm)
GO(21;0)	2.5	2.1	0.02	52
RGO(18;200)	2.5	1.0	0.01	30
RGO(600)	6.6	3.0	0.03	22
G	632	55	3.6	23

amounts to 23 nm, the pore distribution is very broad, a result consistent with the presence of exfoliated graphite layers showing an aerogel-like texture. The GO and RGO samples show low porosity as evidenced by their low BET areas and associated mesoporous volumes. It is evident from the data shown in Table 2 that the reduction of GO in both isothermal mode at 200 °C [in sample RGO(18;200)] and dynamic mode up to 600 °C [RGO(600)] does not change significantly the texture of the material.

Specimen G is characterized by a large BET area which is comparable to other graphene materials reported in the literature [29]. Although this value is sensibly lower than the theoretical surface area of 2630 m^2/g for individual graphene sheets and it is indicative of the existence of ~4 stacked layers, this material is qualitatively and quantitatively different from our RGO's. The nitrogen-adsorption data unequivocally show that the G sample has been exfoliated and that RGO(18;200) and RGO(600) remained primarily stacked. The TEM image for G (see Fig. S4 in the Supplementary Information) shows the expected morphology for an exfoliated specimen containing wrinkles, a result in line with the BET results described above.

3.3. *Nature of polymer-host interactions*

The ability of GO-based materials to intercalate or adsorb PEO is clearly related to their structure and morphology. Based on the results presented so far, Fig. 8 depicts two extreme cases: (a) an intercalated PEO chain between two GO sheets; and (b) PEO chains adsorbed on expanded G sheets. In the first case,

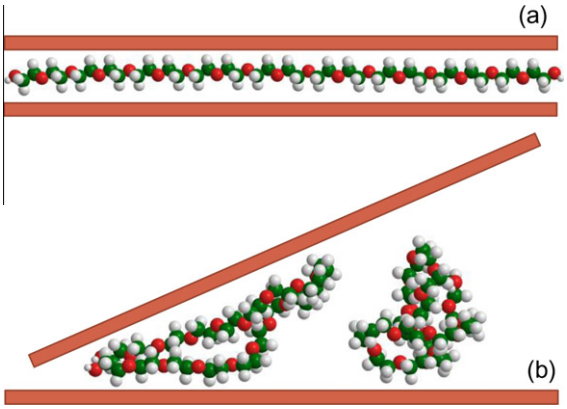

Fig. 8 – Schematic representation of (a) intercalated PEO in GO and (b) adsorbed PEO on thermally reduced/exfoliated GO sheet.

polymer-host interactions are strong as the whole polymer chain is forced to interact with two adjacent GO sheets via both specific (hydrogen bonds linking polymer ether groups and GO hydroxyls) and less specific and weaker interactions (polymer CH_2 - host carbon and oxygen atoms). It is important to note that PEO/GO is confined within a GO interlayer space of 9.2–9.5 Å. Taking into account a thickness of 5.6–5.8 Å for the GO interlayer, the polymer layer amounts to a thickness of about 3.6–3.7 Å. This result implies that PEO is arranged into a two-dimensional monolayer within the GO planes [16,18]. Maximal intercalant uptake is reached when there is one polymer oxygen per GO OH. This simple physical picture explains the observed dependence of polymer uptake on the degree of host oxidation. More importantly, it highlights a suitable strategy to control the chemical composition and properties of graphite-oxide-based polymer intercalates.

In the second case, polymer-host interactions via hydrogen bonds are much weaker as the OH content in the thermally reduced GO samples is extremely low. For instance, the hydrogen (OH) content is ten times lower than in non-reduced GO (see Table 1). Moreover, from our nitrogen physisorption data of G where we find a high pore volume of 3.6 cm^3/g with a broad pore-size distribution (see Fig. S3 in the Supplementary Information), we infer that there exist regions in the material as those schematically depicted in Fig. 8b, which arise from both the expansion of G sheets and the formation of wrinkles on the G surface. In this situation, the topology of the substrate dictates the adsorption of polymer chains, filling the different cavities and re-organizing intra- and inter-molecularly. The interplay between polymer–polymer and polymer-substrate interactions ultimately determines the equilibrium geometry of these macromolecular assemblies as depicted in the figure.

To validate the above physical picture, Fig. 9 shows TM-DSC results for representative PEO/GO and PEO/RGO(G) samples. To aid comparison, TM-DSC data for bulk PEO is also shown in the figure. Bulk PEO shows a large endotherm at 333 K and a small feature at 255 K corresponding to the melting of crystalline regions in PEO, as well as a step at 218 K corresponding to the glass transition of amorphous PEO. On the contrary, PEO/GO and PEO/RGO samples exhibit neither a melting nor a glass-transition associated with the PEO phase, in agreement with previous studies [16–18] as well as with the absence of XRD peaks associated with a PEO crystalline phase. A very different picture emerges for PEO adsorbed onto graphene sheets (PEO/G). In this case, PEO exhibits a clear glass transition (Tg) at 209 K and melting events (Tm) at 304 and 252 K, all noticeably lower than those in the bulk. These large differences can be explained by invoking additional

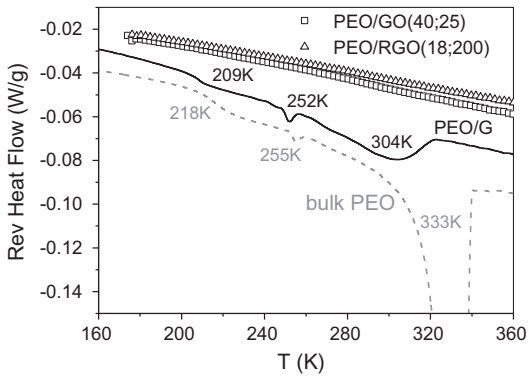

Fig. 9 – TM-DSC data of bulk PEO and representative PEO/GO, PEO/RGO, and PEO/G samples where the intercalated PEO phase shows no signs of glass or melting transitions but, in contrast, the adsorbed PEO on G exhibit well-defined glass and melting transitions at temperatures below those of the bulk phase. For more details on sample composition see Table 1.

conformational flexibility in the adsorbed PEO sample, although the presence of a surface still affects quite noticeably its thermal behaviour, as evidenced by a significant reduction of both Tm and Tg for PEO in PEO/G compared to the bulk. In this scenario, the reduction of accessible chain configurations close to an impenetrable wall lead to the loss of configurational entropy and packing constraints, both of which clearly affect the thermal response of the polymer phase [30].

4. Conclusion

Polymer uptake and intercalation into graphite oxide is a complex process. In this work, we have explored in detail how the chemical composition and structure of a series of graphite-oxide materials exhibiting varying degrees of oxidation and exfoliation affect the uptake of PEO, a ubiquitous polymer. Our results highlight how appropriate control of polymer uptake can be achieved by a judicious choice of the properties of the graphite-oxide host. Specific polymer-host interactions also act to constrain the behaviour of the resulting composite material in a profound way. For PEO, the specific chemical nature (presence of OH groups) in the underlying host above a certain threshold determines both the resulting geometry (e.g., two-dimensional monolayers vs soft macromolecular assemblies) as well as its thermodynamic phase behaviour (e.g., absence or depression of the glass transition). The physical insights gained in this detailed study also provide us with a suitable strategy for the future deployment of a similar methodology to other and more complex polymer systems.

Acknowledgements

The authors gratefully acknowledge the support of the Spanish Ministry of Education (MAT2007-63681), the European Union (502235-2 SOFTCOMP), and the Basque Government (IT-436-07). FBB acknowledges financial support from BERC-MPC. FFA acknowledges financial support from the UK Science and Technology Facilities Council.

Appendix A. Supplementary data

Supplementary data associated with this article can be found, in the online version, at http://dx.doi.org/10.1016/j.carbon.2012.07.008.

REFERENCES

[1] Dreyer DR, Park S, Bielawski CW, Ruoff RS. The chemistry of graphene oxide. Chem Soc Rev. 2010;39(1):228–40.
[2] Giannelis E, Krishnamoorti R, Manias E. Polymer-silicate nanocomposites: model systems for confined polymers and polymer brushes. In: Binder K, de Gennes P-G, Giannelis E, Grest G, Hervet H, et al., editors. Polymers in confined environments. Berlin/Heidelberg: Springer; 1999. p. 107–47.
[3] Cerveny S, Barroso-Bujans F, Alegría A, Colmenero J. Dynamics of water intercalated in graphite oxide. J Phys Chem C 2010;114(6):2604–12.
[4] Barroso-Bujans F, Cerveny S, Alegría A, Colmenero J. Sorption and desorption behavior of water and organic solvents from graphite oxide. Carbon 2010;48(11):3277–86.
[5] Matsuo Y, Niwa T, Sugie Y. Preparation and characterization of cationic surfactant-intercalated graphite oxide. Carbon 1999;37(6). 897-01.
[6] Matsuo Y, Miyabe T, Fukutsuka T, Sugie Y. Preparation and characterization of alkylamine-intercalated graphite oxides. Carbon 2007;45(5):1005–12.
[7] Matsuo Y, Tabata T, Fukunaga T, Fukutsuka T, Sugie Y. Preparation and characterization of silylated graphite oxide. Carbon 2005;43(14):2875–82.
[8] Matsuo Y, Tahara K, Sugie Y. Synthesis of poly(ethylene oxide)-intercalated graphite oxide. Carbon 1996;34(5):672–4.
[9] Matsuo Y, Hatase K, Sugie Y. Preparation and characterization of poly(vinyl alcohol)- and $Cu(OH)_2$-poly(vinyl alcohol)-intercalated graphite oxides. Chem Mater 1998;10(8):2266–9.
[10] Matsuo Y, Tahara K, Sugie Y. Structure and thermal properties of poly(ethylene oxide)-intercalated graphite oxide. Carbon 1997;35(1):113–20.
[11] Bissessur R, Scully SF. Intercalation of solid polymer electrolytes into graphite oxide. Solid State Ionics 2007;178:877–82.
[12] Brodie BC. On the atomic weight of graphite. Philos Trans Roy Soc London. 1859;149:249–59.
[13] Hummers WS, Offeman RE. Preparation of graphitic oxide. J Am Chem Soc 1958;80(6):1339.
[14] Fan X, Peng W, Li Y, Li X, Wang S, Zhang G, et al. Deoxygenation of exfoliated graphite oxide under alkaline conditions: a green route to graphene preparation. Adv Mater 2008;20:4490–3.
[15] Miwa Y, Drews AR, Schlick S. Unique structure and dynamics of poly(ethylene oxide) in layered silicate nanocomposites: accelerated segmental mobility revealed by simulating ESR spectra of spin-labels, XRD, FTIR, and DSC. Macromolecules 2008;41(13):4701–8.
[16] Barroso-Bujans F, Fernandez-Alonso F, Cerveny S, Arrese-Igor S, Alegría A, Colmenero J. Two-dimensional subnanometer confinement of ethylene glycol and poly(ethylene oxide) by neutron spectroscopy: molecular size effects. Macromolecules 2012;45:3137–44.
[17] Barroso-Bujans F, Fernandez-Alonso F, Pomposo JA, Cerveny S, Alegría A, Colmenero J. Macromolecular structure and

vibrational dynamics of confined poly(ethylene oxide): from subnanometer 2D-intercalation into graphite oxide to surface adsorption onto graphene sheets. ACS Macro Lett 2012;1:550–4.
[18] Barroso-Bujans F, Fernandez-Alonso F, Cerveny S, Parker SF, Alegría A, Colmenero J. Polymers under extreme two-dimensional confinement: poly(ethylene oxide) in graphite oxide. Soft Matter 2011;7(16):7173–6.
[19] Barroso-Bujans F, Alegría A, Colmenero J. Kinetic study of the graphite oxide reduction: combined structural and gravimetric experiments under isothermal and nonisothermal conditions. J Phys Chem C 2010;114(49):21645–51.
[20] Brunauer S, Emmett PH, Teller E. Adsorption of gases in multimolecular layers. J Am Chem Soc 1938;60(2): 309–19.
[21] Rouquerol F, Rouquerol J, Sing K. Assessment of surface area. Adsorption by powders and porous solids. London: Academic Press; 1999. p. 165-89.
[22] Harkins WD, Jura G. An absolute method for the determination of the area of a fine crystalline powder. J Chem Phys 1943;11(9):430.
[23] Barrett EP, Joyner LG, Halenda PP. The determination of pore volume and area distributions in porous substances. I. computations from nitrogen isotherms. J Am Chem Soc 1951;73(1):373–80.
[24] Verdejo R, Bernal MM, Romasanta LJ, Lopez-Manchado MA. Graphene filled polymer nanocomposites. J Mater Chem 2011;21(10):3301–10.
[25] Yang D, Velamakanni A, Bozoklu G, Park S, Stoller M, Piner RD, et al. Chemical analysis of graphene oxide films after heat and chemical treatments by X-ray photoelectron and Micro-Raman spectroscopy. Carbon 2009;47(1):145–52.
[26] Bagri A, Mattevi C, Acik M, Chabal YJ, Chhowalla M, Shenoy VB. Structural evolution during the reduction of chemically derived graphene oxide. Nat Chem 2010;2(7):581–7.
[27] Lerf A, He H, Forster M, Klinowski J. Structure of graphite oxide revisited. J Phys Chem B 1998;102(23):4477–82.
[28] Tadokoro H, Chatani Y, Yoshihara T, Tahara S, Murahashi S. Structural studies on polyethers, [–(CH2)m–O–]n. II. molecular structure of polyethylene oxide. Makromol Chem 1964;73(1):109–27.
[29] Srinivas G, Zhu Y, Piner R, Skipper N, Ellerby M, Ruoff R. Synthesis of graphene-like nanosheets and their hydrogen adsorption capacity. Carbon 2010;48(3):630–5.
[30] Baschnagel J, Binder K. On the influence of hard walls on structural properties in polymer glass simulation. Macromolecules 1995;28(20):6808–18.